NJC

PAPER

View Article Online
View Journal

Cite this: DOI: 10.1039/c6nj01936f

Synthesis and molecular structure of arene ruthenium(II) benzhydrazone complexes: impact of substitution at the chelating ligand and arene moiety on antiproliferative activity†

Mohamed Kasim Mohamed Subarkhan,[a] Rengan Ramesh*[a] and Yu Liu[b]

A convenient method for the synthesis of ruthenium(II) arene benzhydrazone complexes (**1–6**) of the general formula [(η^6-arene)Ru(L)Cl] (arene-benzene or *p*-cymene; L-monobasic bidentate substituted indole-3-carboxaldehye benzhydrazone derivatives) has been described. The complexes have been fully characterized *via* elemental analysis, IR, UV-vis, NMR and ESI-MS spectral methods. The solid-state molecular structures of the representative complexes were determined using a single-crystal X-ray diffraction study and the results indicated the presence of a pseudo octahedral (piano stool) geometry. All the complexes were thoroughly screened for their cytotoxicity against human cervical cancer cells (HeLa), human breast cancer cell line (MDA-MB-231) and human liver carcinoma cells (Hep G2) under *in vitro* conditions. Interestingly, the cytotoxic activity of complexes **3**, **4** and **6** is much more potent than cis-platin with low IC_{50} values against all the cancer cell lines tested. Furthermore, the mode of cell death in the MDA-MB-231 cells was assessed *via* AO–EB staining, Hoechst 33258 staining, flow cytometry and comet assay. Furthermore, the results of Western blot analyses suggest that complexes **3** and **6** accumulate preferentially in the mitochondria of MDA-MB-231 cells and induce apoptosis *via* mitochondrial pathways by up-regulating p53 and Bax, and down-regulating Bcl-2.

Received (in Montpellier, France) 21st June 2016,
Accepted 30th September 2016

DOI: 10.1039/c6nj01936f

www.rsc.org/njc

Introduction

Over the past few decades, a large number of cisplatin analogs have been screened as potential antitumor agents, but of these, only two, carboplatin and oxaliplatin, have entered world-wide clinical use.[1] Regardless of the achievements of the current platinum drugs, they are efficient only for a limited range of cancers, some tumors can posses acquired or intrinsic resistance to them and furthermore, they often cause severe side-effects.[2,3] Hence, there is a need for new approaches that are purposefully designed to circumvent these drawbacks. In this regard, ruthenium compounds in the +2 or +3 oxidation state are considered to be suitable candidates for anticancer drug design, since they exhibit a similar spectrum of kinetics for their ligand substitution reactions as platinum(II). A number of ruthenium compounds have been shown to display promising anticancer activities and two ruthenium(III) complexes have entered clinical trials, *trans*-[$RuCl_4$(DMSO)(Im)]ImH (NAMI-A, where Im-imidazole),[4] and *trans*-[$RuCl_4(Ind)_2$]IndH (KP1019), where Ind-indazole.[5]

Several reports have been focused on the anticancer potential of half-sandwich Ru(II) arene complexes of the type [(η^6-arene)Ru(YZ)(X)], where Y and Z are bidentate chelating groups (NN, NO, OO, SO) or two monodentate ligands, and X is a monodentate moiety (often a leaving group *e.g.* Cl). These complexes have been extensively studied as anticancer agents.[6] These half-sandwich "piano-stool" complexes offer great scope for design, with the potential to vary each of the building blocks to allow modification of the thermodynamic and kinetic parameters. Indeed, it has been found that increasing the size of the coordinated arene increases their activity in the human ovarian cancer cell line. Changing the chelating ligand in these ruthenium arene complexes also appears to have an enormous effect on their kinetics and even changes their nucleobase selectivity.[7]

The synthesis and antiproliferative activity of Ru^{II}(η^6-arene) compounds carrying bioactive flavonol ligands have been reported by Hartinger *et al.* (**A**).[8] Wei Su *et al.* have described the DNA binding properties and anticancer activities of ketone N4 substituted thiosemicarbazones and their ruthenium(II)

[a] *Centre for Organometallic Chemistry, School of Chemistry, Bharathidasan University, Tiruchirappalli-620 024, Tamil Nadu, India. E-mail: rrameshbdu@gmail.com*
[b] *Institute of High Energy Physics, Chinese Academy of Sciences, Beijing 100 049, China*

† Electronic supplementary information (ESI) available: Selected crystal data and structure refinement data and figures containing the ^{1}H and ^{13}C NMR, ESI-MS, UV-vis spectrum and intermolecular interaction diagrams of complexes **3** and **6**. CCDC 1499166 (**3**) and 1498893 (**6**). For ESI and crystallographic data in CIF or other electronic format see DOI: 10.1039/c6nj01936f

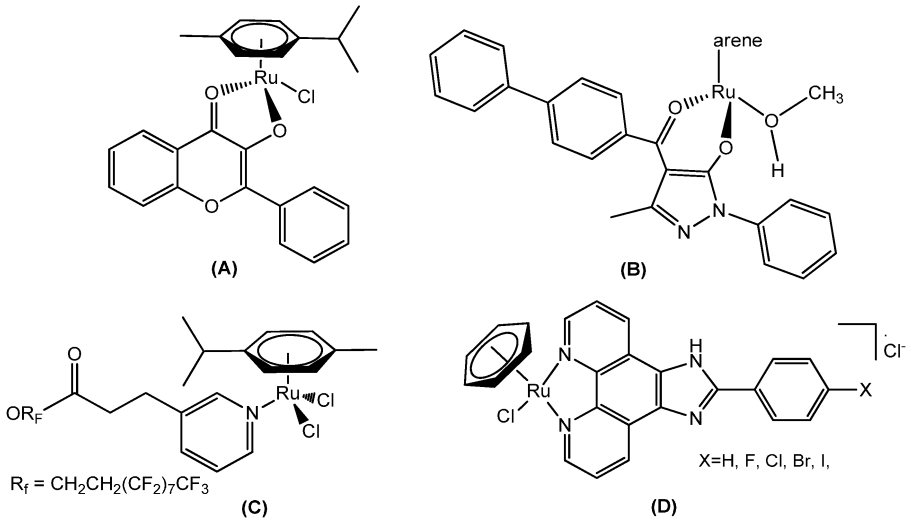

Fig. 1 Reported ruthenium(II) arene anticancer drugs.

arene complexes.[9] A series of ruthenium(II) arene complexes with the 4-(biphenyl-4-carbonyl)-3-methyl-1-phenyl-5-pyrazolonate ligand, and related 1,3,5-triaza-7-phosphaadamantane (PTA) derivatives, have been reported along with their anticancer activities with low IC_{50} values (**B**).[10] Furthermore, Dyson and his co-workers have reported ruthenium(II)–arene complexes with a perfluoroalkyl-modified ligand, which display remarkable *in vitro* cancer cell selectivity (**C**).[11] Recently, the inhibitory activity of ruthenium(II) arene complexes of 2-phenylimidazole[4,5*f*][1,10]phenanthroline against the migration and invasion of MDA-MB-231 breast cancer cells has been investigated (**D**) (Fig. 1).[12]

In recent years, much attention has been given to compounds with pharmacophore hydrazone moieties due to the identification of several hydrazone lead compounds showing antiproliferative[13] and antitumor activities.[14] It has been found from the literature that only a few reports are available on the synthesis, characterisation and cytotoxicity of ruthenium(II) complexes containing hydrazone ligands.[15] Nevertheless, it should be pointed out that, as far as we know, the biological properties of arene ruthenium complexes bearing aroylhydrazones have not been studied so far. Therefore, in this study, we have combined a ruthenium unit with a benzhydrazone ligand to generate a series of organometallic compounds with significant anticancer activities, taking advantage of the synthetic versatility of hydrazone derivatives and their promising biological activities.

We describe here the synthesis and characterization of Ru(II) arene complexes containing bidentate indole-3-carboxaldehyde benzhydrazone ligands and chlorine. All the synthesized complexes have been characterized *via* elemental analysis, IR, UV-vis and NMR and ESI-MS spectroscopy techniques. The molecular structures of complexes **3** and **6** were confirmed through single crystal X-ray diffraction. The *in vitro* cytotoxicity of complexes **1–6** against HeLa, MDA-MB-231, Hep G2 and NIH 3T3 cells were screened using an MTT assay. The morphological changes were investigated using various apoptosis assays (AO–EB staining, Hoechst staining, flow cytometry technique and comet assay). Furthermore, the apoptosis pathway was confirmed by the change in the mitochondrial membrane potential and through western blot analysis.

Experimental section

Methods and instrumentation

The microanalysis of carbon, hydrogen, nitrogen and sulphur was recorded on an analytical function testing Vario EL III CHNS elemental analyser at the Sophisticated Test and Instrumentation Centre (STIC), Cochin University, Kochi. Melting points were recorded with a Boetius micro-heating table and were corrected. Thermal measurements (TGA/DTA) were carried out on a Perkin Elmer Thermal Analyzer under a nitrogen atmosphere with a heating rate of 10 °C min^{-1}. FT-IR spectra were recorded on KBr pellets using a JASCO 400 plus spectrometer. Electronic spectra in chloroform solution were recorded using a CARY 300 Bio UV-visible Varian spectrometer. ^{1}H NMR and ^{13}C-NMR were spectra were recorded on a Bruker 400 MHz instrument using tetramethylsilane (TMS) as the internal reference. A Micro mass Quattro II triple quadrupole mass spectrometer was utilized for electrospray ionization mass spectrometry (ESI-MS). The theoretical calculations were performed using IsoPro software.[16]

Materials

The starting materials $[(\eta^6\text{-}C_6H_6)RuCl_2]_2$ and $[(\eta^6\text{-}p\text{-cymene})RuCl_2]_2$ were prepared according to methods reported in the literature.[17]

Procedure for the preparation of the indole-3-carboxaldehyde benzhydrazone ligands

The ligands L1–L3 were prepared according to the methods reported in the literature.[18] A mixture of 4-substituded benzhydrazide (R = H, Cl or OMe derivatives) (1 mmol) and indole-3-carboxaldehyde (1 mmol) in ethanol (10 mL) containing a drop of glacial acetic acid was refluxed for 30 min. The separated

solid was filtered and dried in air. The ligands were further purified *via* recrystallisation from methanol. Yield: 67–92%.

Procedure for the synthesis of the ruthenium(II) arene benzhydrazone complexes

A mixture containing $[(\eta^6\text{-arene})RuCl_2]_2$ (arene-benzene or *p*-cymene) (0.05 mmol), the indole-3-carboxaldehyde benzhydrazone ligand (0.1 mmol) and triethylamine (0.3 mL) in benzene (20 ml) was created and stirred at room temperature for 2 h. The orange brown precipitate was filtered, washed with hexane and dried *in vacuo*. The reaction progress was monitored using thin layer chromatography.

[Ru(η^6-C_6H_6)(Cl)(L1)] (1). Brown solid. Yield = 0.160 g (68%); m.p.: 180 °C (with decomposition); Calculated: $C_{22}H_{18}ClN_3ORu$: C, 55.40; H, 3.80; N, 8.81%. Found: C, 55.37; H, 3.79; N, 8.82%. IR (KBr, cm^{-1}): 1539 $\nu_{(C=N-N=C)}$, 1490 $\nu_{(N=C-O)}$, 1369 $\nu_{(C-O)}$. UV-Vis (CH_3CN, λ_{max}/nm; ε/dm^3 mol^1 cm^{-1}): 418 (1143), 273 (6371), 227 (14 757). ^1H NMR (400 MHz, $CDCl_3$) (δ ppm): 11.55 (br, 1H, indole N–H), 9.24 (s, 1H, HC═N), 7.08–7.98 (m, 10H, aromatic), 5.72 (s, 6H, CH-benzene). ^{13}C NMR (400 MHz, $CDCl_3$) (δ ppm) 164.15, 131.23, 129.73, 129.52, 129.20, 128.50, 127.50, 127.18, 125.05, 123.45, 122.45, 117.10, 116.82, 87.94 ppm. ESI-MS: displays a peak at *m*/*z* 441.56 $(M - Cl)^+$ (calcd *m*/*z* 442.05).

[Ru(η^6-C_6H_6)(Cl)(L2)] (2). Brown solid. Yield = 0.0933 g (69%); m.p.: 172 °C (with decomposition); Calculated: $C_{22}H_{17}Cl_2N_3ORu$: C, 51.67; H, 3.35; N, 8.22%. Found: C, 51.68; H, 3.36; N, 8.20%. IR (KBr, cm^{-1}): 1531 $\nu_{(C=N-N=C)}$, 1487 $\nu_{(N=C-O)}$, 1378 $\nu_{(C-O)}$. UV-Vis (CH_3CN, λ_{max}/nm; ε/dm^3 mol^1 cm^{-1}): 419 (1044), 269 (4977), 233 (10 051). ^1H NMR (400 MHz, $CDCl_3$) (δ ppm): 11.45 (br, 1H, indole N–H), 9.35 (s, 1H, HC═N), 6.78–7.92 (m, 9H, aromatic), 5.72 (s, 6H, CH-benzene). ^{13}C NMR (400 MHz, $CDCl_3$) (δ ppm) 162.73, 159.67, 130.61, 130.43, 129.30, 128.17, 114.54, 114.12, 88.57 ppm. ESI-MS: displays a peak at *m*/*z* 475.97 $(M - Cl)^+$ (calcd *m*/*z* 476.01).

[Ru(η^6-C_6H_6)(Cl)(L3)] (3). Orange brown solid. Yield = 0.268 g (92%); m.p.: 186 °C (with decomposition); Calculated $C_{23}H_{20}ClN_3O_2Ru$: C, 54.49; H, 3.98; N, 8.29%. Found: C, 54.48; H, 4.00; N, 8.29%. IR (KBr, cm^{-1}): 1530 $\nu_{(C=N-N=C)}$, 1486 $\nu_{(N=C-O)}$, 1376 $\nu_{(C-O)}$. UV-Vis (CH_3CN, λ_{max}/nm; ε/dm^3 mol^1 cm^{-1}): 429 (1496), 268 (4904), 236 (10 242). ^1H NMR (400 MHz, $CDCl_3$) (δ ppm): 11.45 (br, 1H, indole N–H), 9.36 (s, 1H, HC═N), 6.78–8.02 (m, 9H, aromatic), 5.72 (s, 6H, CH-benzene), 3.86 (s, 3H, OCH3). ^{13}C NMR (400 MHz, $CDCl_3$) (δ ppm) 163.98, 136.49, 131.52, 128.90, 128.42, 126.99, 124.97, 12.69, 117.55, 117.00, 114.27, 114.27, 105.82, 88.94, 56.08 ppm. ESI-MS: displays a peak at *m*/*z* 471.99 $(M - Cl)^+$ (calcd *m*/*z* 472.06). Single crystals suitable for X-ray diffraction were obtained *via* recrystallisation in DCM and methanol solution.

[Ru(η^6-*p*-cymene)(Cl)(L1)] (4). Orange-brown solid. Yield = 0.240 g (80%); m.p.: 168 °C (with decomposition); Calculated: $C_{26}H_{26}ClN_3ORu$: C, 58.59; H, 4.92; N, 7.88%. Found: C, 58.59; H, 4.97; N, 7.85%. IR (KBr, cm^{-1}): 1528 $\nu_{(C=N-N=C)}$, 1486 $\nu_{(N=C-O)}$, 1371 $\nu_{(C-O)}$. UV-Vis (CH_3CN, λ_{max}/nm; ε/dm^3 mol^1 cm^{-1}): 431 (1044), 266 (4941), 228 (11 908). ^1H NMR (400 MHz, $CDCl_3$) δ (ppm): 11.86 (br, 1H, indole N–H), 9.29 (s, 1H, HC═N), 6.95–8.33 (m, 10H, aromatic), 5.58 (d, 1H, *p*-cym-H), 5.43 (d, 1H, *p*-cym-H), 5.40 (d, 1H, *p*-cym-H), 5.32 (d, 1H, *p*-cym-H), 2.85 (m, 1H, *p*-cym $CH(CH_3)_2$), 2.31 (s, 3H, *p*-cym CCH_3), 1.28 (d, 3H, *p*-cym $CH(CH_3)_2$), 1.23 (d, 3H, *p*-cym $CH(CH_3)_2$). ^{13}C NMR (400 MHz, $CDCl_3$) (δ ppm) 164.63, 151.89, 147.82, 146.37, 131.61, 131.06, 129.65, 129.38, 128.68, 127.39, 125.25, 123.62, 123.13, 117.2, 116.06, 113.01, 32.25, 29.31, 27.07 ppm. ESI-MS: displays a peak at *m*/*z* 497.62 $(M - Cl)^+$ (calcd *m*/*z* 498.12).

[Ru(η^6-*p*-cymene)(Cl)(L2)] (5). Brown solid. Yield = 0.269 g (82%); m.p.: 176 °C (with decomposition); calculated: $C_{26}H_{25}Cl_2N_3ORu$: C, 55.03; H, 4.44; N, 7.40%. Found: C, 55.06; H, 4.41; N, 7.42%. IR (KBr, cm^{-1}): 1532 $\nu_{(C=N-N=C)}$, 1481 $\nu_{(N=C-O)}$, 1376 $\nu_{(C-O)}$. UV-Vis (CH_3CN, λ_{max}/nm; ε/dm^3 mol^1 cm^{-1}): 410 (1237), 270 (6908), 232 (15 482). ^1H NMR (400 MHz, $CDCl_3$) δ (ppm): 11.86 (br, 1H, indole N–H), 9.39 (s, 1H, HC═N), 6.98–7.62 (m, 9H, aromatic), 5.63 (d, 1H, *p*-cym-H), 5.50 (d, 1H, *p*-cym-H), 5.45 (d, 1H, *p*-cym-H), 5.38 (d, 1H, *p*-cym-H), 3.10 (m, 1H, *p*-cym $CH(CH_3)_2$), 2.34 (s, 3H, *p*-cym CCH_3), 1.40 (d, 3H, *p*-cym $CH(CH_3)_2$), 1.36 (d, 3H, *p*-cym $CH(CH_3)_2$). ^{13}C NMR (400 MHz, $CDCl_3$) (δ ppm) 164.15, 131.23, 129.73, 129.52, 129.20, 128.50, 127.50, 127.18, 125.05, 123.45, 122.45, 117.10, 116.82, 87.94 ppm. ESI-MS: displays a peak at *m*/*z* 531.21 $(M - HCl)^+$ (calcd *m*/*z* 532.08).

[Ru(η^6-*p*-cymene)(Cl)(L3)] (6). Orange-brown solid. Yield = 0.180 g (78%); m.p.: 183 °C (with decomposition); calculated: $C_{27}H_{28}ClN_3O_2Ru$: C, 57.59; H, 5.01; N, 7.46%. Found: C, 57.59; H, 5.01; N, 7.47%. IR (KBr, cm^{-1}): 1530 $\nu_{(C=N-N=C)}$, 1485 $\nu_{(N=C-O)}$, 1372 $\nu_{(C-O)}$. UV-Vis (CH_3CN, λ_{max}/nm; ε/dm^3 mol^1 cm^{-1}): 427 (1576), 269 (7294), 229 (13 110). ^1H NMR (400 MHz, $CDCl_3$) δ (ppm): 11.88 (br, 1H, indole N–H), 9.49 (s, 1H, HC═N), 6.74–8.58 (m, 9H, aromatic), 5.62 (d, 1H, *p*-cym-H), 5.47 (d, 1H, *p*-cym-H), 5.43 (d, 1H, *p*-cym-H), 5.36 (d, 1H, *p*-cym-H), 3.81 (s, 3H, OCH3), 2.89 (m, 1H, *p*-cym $CH(CH_3)_2$), 2.34 (s, 3H, *p*-cym CCH_3), 1.41 (d, 3H, *p*-cym $CH(CH_3)_2$), 1.37 (d, 3H, *p*-cym $CH(CH_3)_2$). ^{13}C NMR (400 MHz, $CDCl_3$) (δ ppm) 164.21, 147.73, 142.18, 132.99, 131.73, 131.66, 131.40, 130.01, 129.12, 128.40, 127.65, 127.65, 127.12, 126.88, 124.94, 123.98, 117.44, 117.07, 32.16, 29.36, 27.14 ppm. ESI-MS: displays a peak at *m*/*z* 527.86 $(M - Cl)^+$ (calcd *m*/*z* 528.13). Single crystals suitable for X-ray diffraction were obtained *via* recrystallisation in DCM and methanol solution.

X-ray crystallography

Single crystals of $[Ru(\eta^6\text{-}C_6H_6)(Cl)(L3)]$ (**3**) and $[Ru(\eta^6\text{-}p\text{-cymene})(Cl)(L3)]$ (**6**) were grown *via* slow evaporation of the dichloromethane-methanol solution at room temperature. A single crystal of suitable size was covered with Paratone oil, mounted on the top of a glass fiber, and transferred to a Bruker AXS Kappa APEX II single crystal X-ray diffractometer using monochromated MoKα radiation (λ = 0.71073). Data were collected at 293 K. The structure was solved with a direct method using SIR-97 and was refined *via* a full matrix least-squares method on F^2 with SHELXL-97.[19] Non-hydrogen atoms were refined with anisotropic thermal parameters. All hydrogen atoms were geometrically fixed and collected to refine using a riding model. Frame integration and data reduction were performed using Bruker SAINT Plus (Version 7.06a) software. The multi scan absorption corrections were applied to the data using SADABS software. Fig. 1 was

drawn with ORTEP[20] and the structural data were deposited at the Cambridge Crystallographic Data Centre: CCDC 1499166 and 1498893.

Stability studies

The stabilities of complexes **1–6** were checked by recording their UV-visible spectra by dissolving them in a minimum amount of 1% DMSO and then diluting the sample with PBS buffer. The hydrolysis profiles of these complexes were recorded by monitoring the electronic spectra for the resulting mixture over 24 h.

Partition coefficients determination

The hydrophobicity values of complexes **1–6** were measured using the "Shake flask" method in octanol–water phase partitions as reported earlier. Complexes **1–6** (1 mg mL^{-1}) were dissolved in a mixture of water and *n*-octanol (2, 4, 6, 8, 10 μg mL^{-1}) followed by shaking for 1 hour. The mixture was allowed to settle over a period of 30 minutes and the resulting two phases were collected separately without cross contamination of one solvent layer into another. The concentration of the complexes in each phase was determined using UV-Vis absorption spectroscopy at room temperature. The results are given as the mean values obtained from three independent experiments. The sample solution concentration was used to calculate log *P*. The partition coefficients for **1–6** were calculated using the equation log *P* = log[(**1–6**)oct./(**1–6**)aq.].

Cell culture and inhibition of cell growth

Cell culture. HeLa (human cervical cancer cell line), MDA-MB-231 (triple negative breast carcinoma cell line), Hep G2 (human liver carcinoma cell line) and NIH 3T3 (noncancerous cell line, mouse embryonic fibroblast) were obtained from the National Centre for Cell Science (NCCS), Pune. These cell lines were cultured as a monolayer in RPMI-1640 medium (Biochrom AG, Berlin, Germany), supplemented with 10% fetal bovine serum (Sigma-Aldrich, St. Louis, MO, USA), and with 100 U mL^{-1} penicillin and 100 μg mL^{-1} streptomycin as antibiotics (Himedia, Mumbai, India), at 37 °C in a humidified atmosphere of 5% CO_2 in a CO_2 incubator (Heraeus, Hanau, Germany).

Inhibition of cell growth

The IC_{50} values, which are the concentrations of the tested compounds that inhibit 50% of cell growth, were determined using a 3-(4,5-dimethyl thiazol-2yl)-2,5-diphenyl tetrazolium bromide (MTT) assay. Cells were plated in their growth medium at a density of 5000 cells per well in 96 flat bottomed well plates. After 24 h, the benzhydrazone ligands and Ru(II) arene benzhydrazone complexes **1–6** were added at different concentrations (1–250 μM) for 24 h to study the dose dependent cytotoxic effects. To each well, 20 μL of 5 mg mL^{-1} MTT in phosphate-buffer (PBS) was added. The plates were wrapped with aluminium foil and incubated for 4 h at 37 °C. The purple formazan product was dissolved by the addition of 100 μL of 100% DMSO to each well. The quantity of formazan formed gave a measure of the number of viable cells. HeLa, MDA-MB-231 and Hep G2 were used for the MTT assay. The absorbance was monitored at 570 nm (measurement) and 630 nm (reference) using a 96 well plate reader (Bio-Rad, Hercules, CA, USA). Data were collected for four replicates each and used to calculate the respective means. The percentage of inhibition was calculated, from this data, using the formula: Percentage inhibition = 100 × {Mean OD of untreated cells (control) − Mean OD of treated cells}/{Mean OD of untreated cells (control)}. The IC_{50} value was determined as the complex concentration that is required to reduce the absorbance to half that of the control.

Acridine orange and ethidium bromide staining experiment

We observed the changes in chromatin organization in the MDA-MB-231 cells after treatment with IC_{50} concentrations of complexes **3** and **6** by using acridine orange (AO) and ethidium bromide (EB). Briefly, about 5×10^5 cells were allowed to adhere overnight on a coverslip placed in each well of a 12-well plate. The cells were allowed to recover for 1 h, washed thrice with DPBS, stained with an AO and EB mixture (1 : 1, 10 μM) for 15 min, and observed with an epifluorescence microscope (Carl Zeiss, Germany).

Hoechst 33258 staining method

Hoechst 33258 staining was done using the method described earlier with slight modifications. 5×10^5 MDA-MB-231 cells were treated with IC_{50} concentrations of complexes **3** and **6** for 24 h in a 6-well culture plate and were fixed with 4% paraformaldehyde followed by permeabilization with 0.1% Triton X-100. Cells were then stained with 50 μg mL^{-1} Hoechst 33258 for 30 min at room temperature. The cells undergoing apoptosis, represented by the morphological changes of apoptotic nuclei, were observed and imaged using an epifluorescence microscope (Carl Zeiss, Germany).

Apoptosis evaluation – flow cytometry

The MDA-MB-231 cells were grown in a 6-well culture plate and exposed to IC_{50} concentrations of complexes **3** and **6** for 24 h. The Annexin V-FITC kit uses annexin V conjugated with fluorescein isothiocyanate (FITC) to label the phosphatidylserine sites on the membrane surface of apoptotic cells. Briefly, the cells were trypsinised and washed with Annexin binding buffer and incubated with Annexin V-FITC and PI for 30 minutes and immediately analysed using flow cytometer FACS Aria-II. The results were analysed using DIVA software and the percentage of positive cells was calculated.

Cellular DNA damage quantified using the comet assay

DNA damage was quantified by means of the comet assay as described. Assays were performed under red light at 4 °C. Cells used for the comet assay were sampled from a monolayer during the growing phase, 24 h after seeding. MDA-MB-231 cells were treated with complexes **3** and **6** at the IC_{50} concentration, and the cells were harvested using a trypsinization process at 24 h. A total of 200 μL of 1% normal agarose in PBS at 65 °C was dropped gently onto a fully frosted microslide, covered immediately with a coverslip, and placed over a frozen

ice pack for about 5 min. The coverslip was removed after the gel had set. The cell suspension from one fraction was mixed with 1% low-melting agarose at 37 °C in a 1 : 3 ratio. A total of 100 μL of this mixture was applied quickly on top of the gel, coated over the microslide, and allowed to set as before. A third coating of 100 μL of 1% low-melting agarose was placed on the gel containing the cell suspension and allowed to set. Similarly, slides were prepared (in duplicate) for each cell fraction. After solidification of the agarose, the coverslips were removed, and the slides were immersed in an ice-cold lysis solution (2.5 M NaCl, 100 mM Na_2EDTA, 10 mM Tris, NaOH; pH 10, 0.1% Triton X-100) and placed in a refrigerator at 4 °C for 16 h. All of the above operations were performed in low-lighting conditions in order to avoid additional DNA damage. Slides, after removal from the lysis solution, were placed horizontally in an electrophoresis tank. The reservoirs were filled with an electrophoresis buffer (300 mM NaOH and 1 mM Na_2EDTA, pH > 13) until the slides were just immersed in it. The slides were allowed to stand in the buffer for about 20 min (to allow DNA unwinding), after which electrophoresis was carried out at 0.8 V cm^{-1} for 15 min. After electrophoresis, the slides were removed, washed thrice in a neutralization buffer (0.4 M Tris, pH 7.5), and gently dabbed to dry. Nuclear DNA was stained with 20 μL of EB (50 μg mL^{-1}). Photographs were taken using an epifluorescence microscope (Carl Zeiss).

Mitochondrial membrane potential assay

Mitochondrial membrane potential, $\Delta\psi_m$ is an important parameter of mitochondrial function used as an indicator of cell health. MDA-MB-231 cells treated overnight with IC_{50} concentrations of complexes **3** and **6** in 6-well plates were incubated for 1 h with 2 μg mL^{-1} of JC-1 in the culture medium. The adherent cell layer was then washed three times with PBS and dislodged with 250 μL of trypsin–EDTA. Cells were collected in PBS/2% bovine serum albumin (BSA), washed twice *via* centrifugation, resuspended in 0.3 mL of PBS/2% BSA, mixed gently, and examined using a fluorescence microscope (Carl Zeiss, Jena, Germany).

Western blot analysis

For Western blot analysis, MDA-MB-231 cells were treated with complexes **3** and **6** at the IC_{50} concentrations for 24 h, and appropriate amounts of the cell lysates (25 μg protein) were resolved over a 10% Tris-glycine polyacrylamide gel, and then transferred onto the PVDF membrane. The blots were blocked using 5% non-fat dry milk and probed using p53, Bcl-2 and Bax primary monoclonal antibodies in blocking buffer overnight at 4 °C. The membrane was then incubated with the appropriate secondary antibody-horseradish peroxidase conjugate (Amersham Life Sciences Inc., IL, USA), followed by detection using a chemiluminescence ECL kit (Amersham Life Sciences Inc., IL, USA). To ensure equal loading of the protein, the membrane was stripped and reprobed with anti-β-actin antibody (Sigma Aldrich, USA).

Results and discussion

Synthesis of the ruthenium(II) arene benzhydrazone complexes

The hydrazone ligand derivatives were conveniently prepared in an excellent yield *via* condensation of indole-3-carboxaldehyde with 4-substituted benzhydrazides (H, Cl and OMe derivatives) in an equimolar ratio.[17] These ligands were allowed to react with the ruthenium(II) arene precursor $[(\eta^6\text{-arene})RuCl_2]_2$ (arene-benzene or *p*-cymene) in a 2 : 1 molar ratio in the presence of triethylamine as the base and the new complexes of the general formula, $[(\eta^6\text{-arene})Ru(L)Cl]$ (arene-benzene or *p*-cymene; L-substituted indole-3-carboxaldehye benzhydrazone derivatives) (Scheme 1) were obtained in high yields. The addition of triethylamine to the reaction mixture was used to remove a proton from the imidol oxygen and to facilitate the coordination of the imidolate oxygen to the ruthenium(II) ion. All complexes are air-stable and are highly soluble in most organic solvents. The analytical data of all the ruthenium(II) arene benzhydrazone complexes are in good agreement with the molecular formula proposed.

Characterization of the complexes

The IR spectra of the free ligands displayed a medium to strong band in the region of 3180–3196 cm^{-1} which is characteristic of the N–H functional group. The free ligands also displayed $\nu_{C=N}$ and $\nu_{C=O}$ absorptions in the region of 1548–1576 cm^{-1} and 1610–1653 cm^{-1} respectively, which indicate that the ligands exist in the amide form in the solid state. Bands that are due to

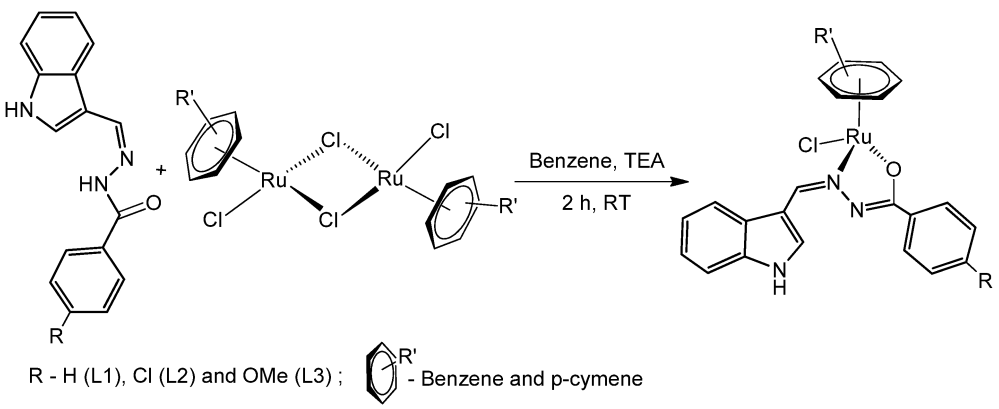

Scheme 1 Synthesis of ruthenium(II) arene indole-3-carboxaldehyde benzhydrazone complexes.

ν_{N-H} and $\nu_{C=O}$ stretching vibrations were not observed with the complexes, which indicates that the ligands underwent tautomerization and subsequent coordination of the imidolate enolate form during complexation. Coordination of the ligand to the ruthenium(II) ion through an azomethine nitrogen is expected to reduce the electron density in the azomethine link, and thus lower the absorption frequency upon complexation to 1528–1539 cm^{-1} which indicates the coordination of azomethine nitrogen to the ruthenium(II) ion. The band in the region of 1369–1378 cm^{-1} is due to the imidolate oxygen, which is coordinated to the metal. The IR spectra of all the complexes therefore confirm the mode of coordination of the benzhydrazone ligand to the ruthenium(II) ion *via* the azomethine nitrogen and imidolate oxygen.[21]

The absorption spectra of the ruthenium(II) arene benzhydrazone complexes in chloroform exhibited very intense bands around 266–273 nm and 227–236 nm, which are assigned to the ligand-centered (LC) π–π* and n–π* transitions, respectively. The lowest energy absorption bands in the electronic spectra of the complexes in the visible region 410–431 nm are ascribed to MLCT (metal to ligand charge transfer) transitions. Based on the pattern of the electronic spectra of all the complexes, an octahedral environment around the ruthenium(II) ion has been proposed similar to that of other octahedral ruthenium(II) arene complexes.[22]

The ^{1}H NMR spectra of all the complexes were recorded in $CDCl_3$ to confirm the bonding of the benzoylhydrazone ligand to the ruthenium(II) ion. The multiplets observed in the region δ 6.74–8.61 ppm in the complexes have been assigned to the aromatic protons of the benzhydrazone ligands. The signal due to the azomethine proton appears in the region δ 9.24–9.49 ppm. The position of the azomethine signal in the complexes is slightly downfield in comparison with that of the free ligand, suggesting deshielding of the azomethine proton due to its coordination to ruthenium. The singlet due to the –NH proton of the free ligand in the region δ 11.22–11.60 ppm is absent in the complex, further supporting enolisation and coordination of the imidolate oxygen to the Ru(II) ion. Therefore, the ^{1}H NMR spectra of the complexes confirm the bidentate coordination mode of the benzhydrazone ligands to the ruthenium(II) ion. In all the complexes, the indole N–H protons are observed as singlets in between δ 11.41–11.88 ppm. The cymene protons appeared in the region of δ 5.32–5.62 ppm.[23] In addition, the two isopropyl methyl protons of the *p*-cymene appeared as two doublets in the region of δ 1.23–1.41 ppm, and the methine protons appeared in the region of δ 2.31–3.10 ppm as septets. Furthermore, the methyl group of the *p*-cymene appeared as a singlet around the region of δ 2.31–2.34 ppm. Additionally, the methoxy protons are observed as singlets for complexes **3** and **6** at δ 3.81–3.86 ppm. On the other hand, the benzene arene protons displayed an upfield shift relative to complex **4–6** in the region δ 5.72–5.73 ppm (Fig. S1, ESI†). The ^{13}C NMR of the Ru(II) arene complexes showed resonance in the expected regions (Fig. S2, ESI†), and the complex revealed a downfield shift of the azomethine carbon relative to the free ligands, indicating coordination of the azomethine nitrogen to the metal centre.

Stability of the complexes (time-dependent spectra)

Stability in solution is an important requirement for drug candidates. The stability of the most cytotoxic complexes **1–6**, was studied using UV-Vis spectroscopy in a solution of 1% DMSO in PBS. All the ruthenium(II) arene benzhydrazone complexes showed characteristic peaks in the region of 200–800 nm and did not exhibit any significant changes during a 24 hour period. The absence of significant changes in the peak absorptions and spectral characteristics for the tested complexes over time may suggest that no structural alternations occurred in buffer solution. The data for all the studied complexes are presented in Fig. S5 (ESI†). Furthermore, the composition of the complexes has been studied *via* ESI-MS spectral studies. Mass spectrometric measurements were carried out under a positive ion ESI mode using acetonitrile as the solvent. Their positive ESI mass spectra **1–6** showed major peaks due to the cationic fragment $[(\eta^6\text{-arene})Ru(L)Cl]^+$ generated by loss of the Cl^-. The ESI spectra of complexes **1–6** display *m*/*z* found (calcd): [441.56 (442.05) (1, M − Cl)$^+$], [475.97 (476.01) (2, M − Cl)$^+$], [471.99 (472.06) (3, M − Cl)$^+$], [497.62 (498.12) (4, M − Cl)$^+$], [531.21 (532.08) (5, M − HCl)$^+$] and [527.86 (528.13) (6, M − Cl)$^+$], respectively confirming the presence of a monomeric entity in the solution phase. The mass spectrometry results are in good agreement with the proposed molecular formulae of the complexes and suggest that the chloro (Cl^-) group is labile and possibly replaced by the targeted biomolecules. The experimentally observed and theoretically calculated isotopic distributions were in excellent agreement with each other as shown in Fig. S3 and S4 (ESI†). Furthermore, the thermal stability of the synthesized ruthenium(II) arene complexes **3** and **6** was determined using thermogravimetric analysis (TGA) and differential thermal analysis (DTA) as shown in Fig. S6 (ESI†). The synthesized complex is stable up to 180 °C. The results are in good agreement with the formulae suggested from the analytical data.

X-ray crystallographic studies

Attempts were made to grow single crystals for all the complexes to confirm the coordination mode of the ligand to metal and the geometry of the complex. However, we obtained single crystals for complexes $[Ru(\eta^6\text{-}p\text{-cymene})(Cl)(L3)]$ (**3**) and $[Ru(\eta^6\text{-}C_6H_6)(Cl)(L3)]$ (**6**). Crystals of **3** and **6** grew from the slow diffusion of dichloromethane into methanol solutions and crystallized in the monoclinic system with a $P2(1)/n$ space group. The selected bond lengths and bond angles are given in Table 1, whereas the crystallographic data and structural refinement parameters are gathered in Table S1 (ESI†). The ORTEP views of the molecules with atom numbering are shown in Fig. 2 and 3. The molecular structure of complex **3** shows clearly that the benzhydrazone ligand coordinates in a bidentate manner to the ruthenium ion *via* the azomethine nitrogen and imidolate oxygen in addition to one chlorine and one arene group. The complex adopts the commonly observed piano-stool geometry as reported in many half-sandwich arene ruthenium(II) complexes.[24] In this case, the arene ring forms the seat of the piano-stool, while the bidentate benzhydrazone N, O and Cl

Table 1 Selected bond lengths (Å) and angles (°) in **3**·H_2O and **6**

Distances/angles	**3**·H_2O	**6**
Ru1–N2	2.069(3)	2.077(4)
Ru1–O1	2.069(3)	2.065(4)
Ru1–Cl1	2.4233(13)	2.4060(16)
Ru1–C22	2.156(7)	2.153(5)
N1–N2	1.391(5)	1.389(6)
N2–C7	1.326(6)	1.326(6)
O2–C9	1.289(5)	1.289(6)
O1–Ru1–N2	76.18(12)	75.71(16)
N2–Ru1–Cl1	84.26(11)	83.85(13)
N2–N1–Ru1	116.0(2)	115.7(3)
C7–O1–Ru1	112.8(2)	112.8(3)
C7–N2–N1	110.5(3)	110.6(4)
C19–Ru1–Cl1	106.2 (3)	104.81(16)
O1–Ru1–Cl1	84.46(10)	86.90(12)

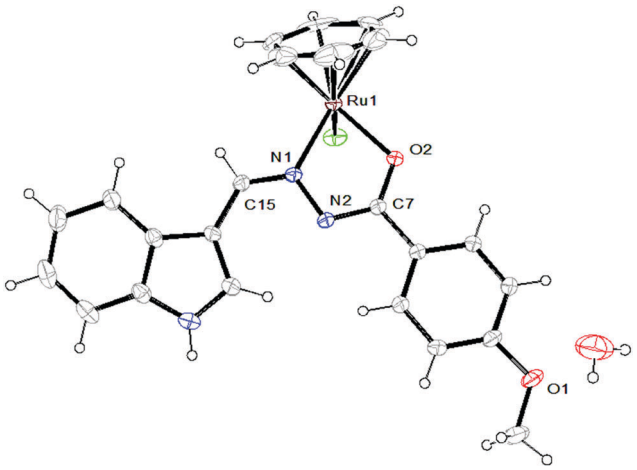

Fig. 2 ORTEP drawing of complex **3**·H_2O at 30% probability level.

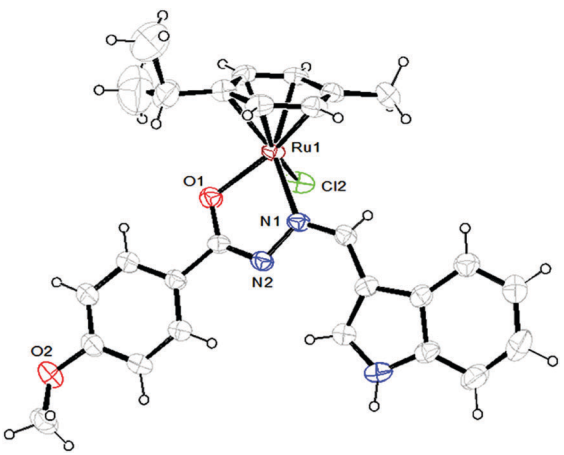

Fig. 3 ORTEP drawing of complex **6** at 30% probability level.

ligands form the three legs of the stool. Therefore, the ruthenium(II) ion is sitting in a NOCl (η^6-arene) coordination environment. The benzhydrazone ligand binds to the metal centre at N and O forming the five membered chelate ring with a bite angle of 76.18(12)° O(1)–Ru(1)–N(2) and 84.26(11)° N(2)–Ru(1)–Cl(1). The bond lengths of Ru(1)–N(2) and Ru(1)–O(1) are 2.069(3) and 2.069(3) Å, respectively. The Ru–Cl bond length is found to be 2.4233(13) Å and the bond length is in agreement with other structurally characterized *p*-cymene ruthenium complexes.[25] The ruthenium atom is π bonded to the arene ring with an average Ru–C distance of 2.156(7) Å, whereas the average C–C bond length in the arene ring is 1.425(8) Å, with alternating short and long bonds. It was observed that complex **6** also adopts a similar geometrical environment as in complex **3** with slight variation in the bond angles and bond distances. The crystal structures of **3** and **6** revealed the presence of extensive intermolecular hydrogen bonding interactions as shown in Fig. S7, ESI†.

Partition coefficient determination

Lipophilicity is an important factor for the cellular accumulation and oral bioavailability of drugs. It is often expressed as the *n*-octanol/water partition coefficient (log *P*), which is also a central parameter in many *in silico* medicinal chemistry approaches, such as the determination of the drug likeliness of a new drug. This was investigated by the partition coefficient, *P*, a parameter which indicates the hydrophobic character of molecules and their ability to cross lipid bilayers.[26] The calculated log *P* values for complexes **1**–**6** are 2.59, 2.72, 2.48, 2.23, 2.35 and 1.99 respectively. It has been observed that complex **6** with a *p*-cymene group shows a higher potency than the rest of the complexes (Table 2).

In vitro antiproliferative activity

All the ruthenium complexes and the free benzhydrazone ligands were evaluated for their cytotoxic activity against HeLa, MDA-MB-231 and Hep-G2 along with NIH 3T3 cell lines by using a colorimetric assay (MTT assay) that measures mitochondrial dehydrogenase activity as an indication of cell viability. The effects of the ruthenium(II) arene complexes to arrest the proliferation of cancer cells were evaluated after exposure for 24 h. It is to be noted that the ligands did not show any inhibition of the cell growth even up to 100 μM and clearly indicates that chelation of the ligand with the metal ion is responsible for the observed cytotoxicity properties of the complexes. The results of the MTT assays revealed that the complexes showed notable

Table 2 Cytotoxicity (IC_{50}, μM) of the ligands and complexes **1**–**6**. (n.e.: no effect) and their calculated partition coefficients (log *P*)

	IC_{50} values (μM)				
Complex	HeLa	MDA-MB-231	Hep G2	NIH3T3	log *P*
Complex **1**	20.8 ± 0.2	18.2 ± 0.8	14.2 ± 0.3	223.9 ± 0.7	2.59 ± 0.4
Complex **2**	25.9 ± 0.8	19.9 ± 0.1	16.8 ± 0.5	215.3 ± 0.6	2.72 ± 0.3
Complex **3**	19.4 ± 0.3	15.3 ± 0.3	13.4 ± 0.4	235.4 ± 0.3	2.48 ± 0.3
Complex **4**	13.6 ± 0.4	11.2 ± 0.3	11.6 ± 0.4	230.4 ± 0.5	2.23 ± 0.2
Complex **5**	17.9 ± 0.3	12.8 ± 0.2	12.8 ± 0.1	224.3 ± 0.8	2.35 ± 0.3
Complex **6**	11.4 ± 0.7	4.1 ± 0.4	9.1 ± 0.3	241.3 ± 0.4	1.99 ± 0.2
L1	n.e.	n.e.	n.e.	n.e.	
L2	n.e.	n.e.	n.e.	n.e.	
L3	n.e.	91.7 ± 0.5	94.7 ± 0.9	n.e.	
Cisplatin	19.2 ± 1.1	12.9 ± 0.6	20.1 ± 1.2	212.3 ± 0.6	

The ligands L1–L3 were added at different concentrations (1–250 μM) for 24 h.

activity against the cell lines HeLa, MDA-MB-231 and Hep-G2 with respect to the IC_{50} values (Table 2). From the IC_{50} values obtained, it was inferred that complexes **3**, **4** and **6** are highly active against all the cell lines with very low IC_{50} values compared with the values for the well-known anticancer drug cisplatin. In addition, the *in vitro* cytotoxic activity studies of the complexes against the mouse embryonic fibroblast cell line NIH 3T3 (normal cells) was undertaken and the IC_{50} values are above 215 μM, which confirms that the complexes are very specific to cancer cells.

These ruthenium(II) arene benzhydrazone complexes **1–6** posses significant cytotoxicity over the ligands, which may be due to the presence of extended π conjugation resulting from the chelation of Ru(II) ions with the ligand. Furthermore, the observed higher activity of complexes **4** and **6** is correlated to the nature of the chelating benzoylhydrazone ligand and arene moiety. Additionally, the observed higher activity of complexes **3** and **6** is correlated to the nature of the chelating benzhydrazone ligand and arene moiety. In complexes **3** and **6**, the presence of an electron donating methoxy substituent at the phenyl ring of the ligand increases the lipophilic character of the metal complex, which favours its permeation through the lipid layer of a cell membrane.

On the other hand, the arene groups also play an important role in the antitumor activity of these ruthenium complexes. It has been observed that complex **6** with a *p*-cymene group shows higher potency than those with a benzene group in complex **3**, which may be attributed to the stronger hydrophobic interactions between the Ru(II)–cymene complex and the biomolecular targets as evidenced by the partition coefficient value.[27] Complex **6** shows a high cytotoxic activity with very low IC_{50} values of 11.4 ± 0.7, 4.1 ± 0.4 and 9.1 ± 0.3 μM toward HeLa, MDA-MB-231 and Hep-G2. Furthermore, the IC_{50} values are much better than those previously reported for other Ru(II) arene arylazo, 2-thiosalicylic acid, phenanthroimidazole or polypyridyl complexes.[10,28] These excellent results suggest further investigation of the underlying mechanism accounting for the antiproliferative action of these ruthenium arene benzhydrazone complexes is warranted.

AO–EB and Hoechst staining assays

Acridine orange and ethidium bromide (AO and EB) dual staining followed by fluorescence microscopy revealed apoptosis from the perspective of fluorescence emission. Apoptosis is characterized by cell shrinkage, blebbing of the plasma membrane and chromatin condensation. To identify apoptosis, at a basic level, we adopted AO–EB staining to visualize and quantify the number of viable and apoptic cells. According to the difference in membrane integrity between necrotic and apoptosis, AO can pass through a cell membrane, but EB cannot. The apoptotic effect after the treatment of MDA-MB-231 cells with complexes **3** and **6** for 24 h at IC_{50} concentrations is shown in Fig. 4. The cells incubated with complexes **3** and **6** for 2 h and irradiated with visible light showed the significant reddish-orange emission characteristic of apoptotic cells. In the control, the cells of MDA-MB-231 were stained bright green in spots. Additionally, complexes **3** and **6** treated MDA-MB-231 cells were stained with Hoechst 33258, and apoptotic features such as nuclear shrinkage and chromatin condensation were also observed (Fig. 5). Hence the results of AO–EB and Hoechst staining assays suggest that complexes **3** and **6** induce apoptosis in MDA-MB-231 cells.[28,29]

Evaluation of apoptosis – flow cytometry

The potential to induce apoptosis in cancer cells by the addition of synthesized complexes can be quantitatively investigated using flow cytometry analysis and the Annexin V protocol, with the help of Annexin V-FITC Apoptosis Detection Kit to perform double-staining with propidium iodide and Annexin V-FITC. Annexin V, a Ca^{2+} dependent phospholipid-binding protein with a high affinity for the membrane phospholipid phosphatidylserine (PS), is quite helpful for identifying apoptotic cells with exposed PS. Propidium iodide is a standard flow cytometric viability probe used to distinguish viable from non-viable cells (Fig. 6). The MDA-MB-231 cells were treated with complexes **3** and **6** at IC_{50} concentrations for 24 h. The cell death induced by the complexes follows a pathway from the lower left quadrant to the upper right quadrant (Annexin V^+/PI^+) which represents cells undergoing apoptosis.[30]

Comet assay

The comet assay (single-cell gel electrophoresis) in an agarose gel matrix was used to study DNA fragmentation. When the comet assay was performed with treated MDA-MB-231 cancer cells with IC_{50} concentrations of complexes **3** and **6**, large and well-rounded comets were observed, while the control cells failed to show a comet like appearance (Fig. 7). The comet

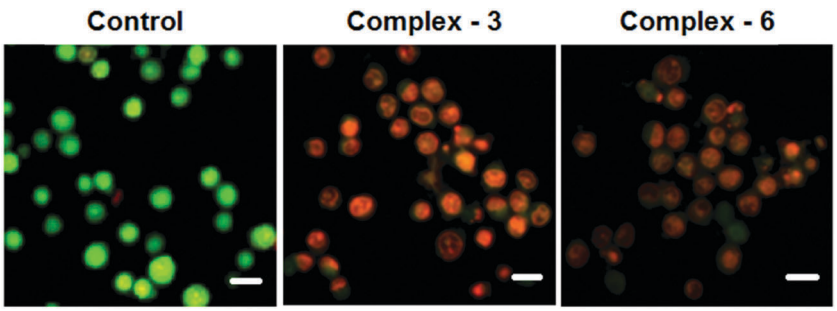

Fig. 4 Morphological assessment of AO and EB of MDA-MB-231 cells treated with complexes **3** and **6** (at IC_{50} concentrations) for 24 h. The scale bar 20 μm.

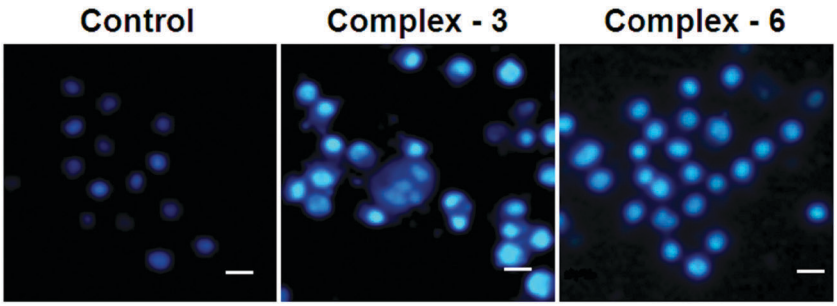

Fig. 5 Morphological assessment of complexes **3** and **6** (at IC_{50} concentrations) and MDA-MB-231 cells for 24 h. The scale bar 20 μm.

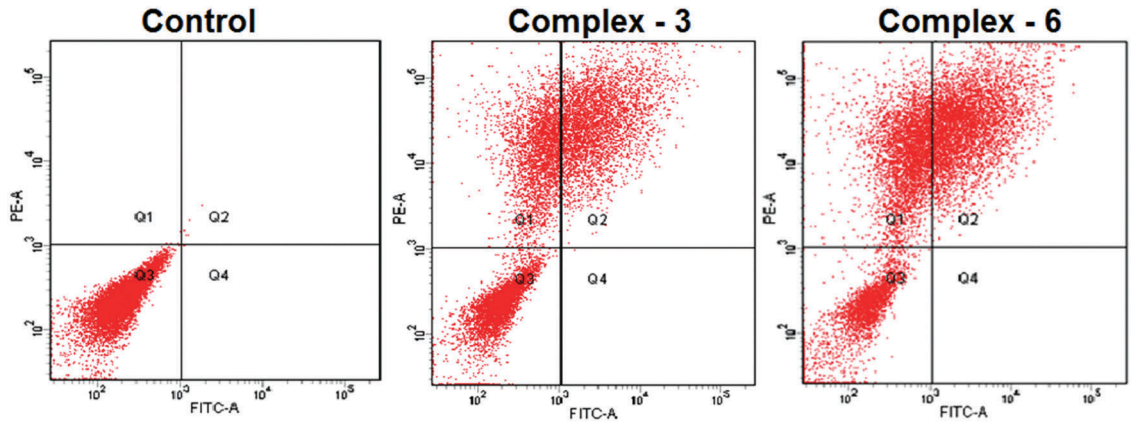

Fig. 6 AnnexinV/propidium iodide assay of MDA-MB-231 cells treated with complexes **3** and **6** (at IC_{50} concentrations) measured using flow cytometry.

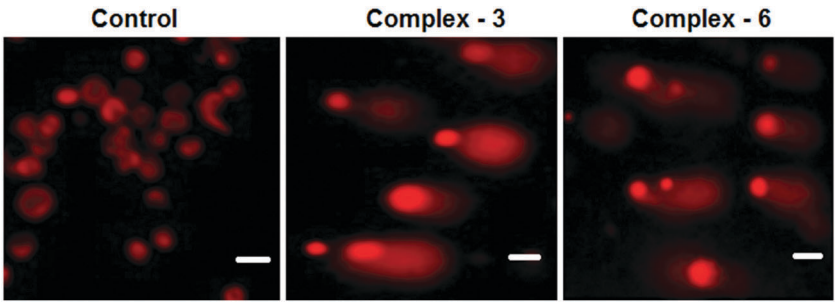

Fig. 7 Comet assay of staining of the EB control (untreated) treated with complexes **3** and **6** (at IC_{50} concentrations) for 24 h. The scale bar 40 μm.

score for complexes **3** and **6** shows a significant number of nucleoids with larger comet tails, indicative of higher levels of DNA single-strand breaks.[31]

Mitochondrial membrane potential detection

Mitochondria act as a point of integration for apoptotic signals originating from both extrinsic and intrinsic apoptotic pathways. Mitochondria play important roles in apoptosis through the release of proapoptotic factors such as cytochrome *c* and other apoptosis-inducing factors. The changes in the mitochondrial membrane potential were detected using the fluorescent probe JC-1. It exhibits potential-dependent accumulation in mitochondria, indicated by a fluorescence emission shift from red (~590 nm) to green (~525 nm). As shown in Fig. 8, in the control, JC-1 emits red fluorescence. When the MDA-MB-231 cells were treated with the complexes, JC-1 displays a green fluorescence. The changes from red to green fluorescence indicate the decrease of mitochondrial membrane potential (Fig. 8). These results suggest that complexes **3** and **6** can induce a decrease in mitochondrial membrane potential.[32]

Western blot analysis

To reveal the underlying mechanism behind the antiproliferative activity of the Ru(II) benzhydrazone complexes, the Western blot technique was utilized. It is established that apoptic proteins like p53, Bax and anti-apoptotic protein Bcl-2 play a pivotal role during the induction of apoptosis. The expression levels of p53, Bax and Bcl-2 proteins were analyzed in the **3** and **6** treated MDA-MB-231 cells and control cells. It was observed that the expression level of the Bcl-2 protein decreases suggesting that

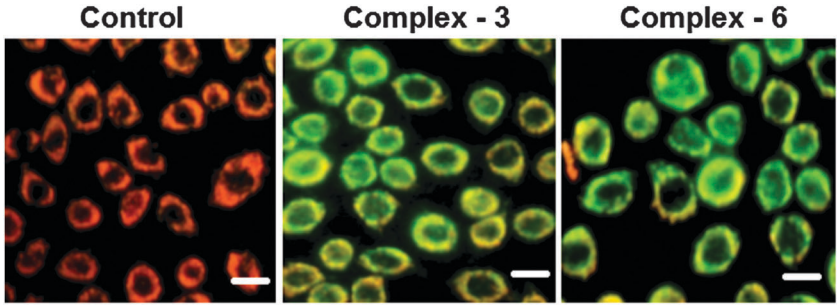

Fig. 8 MDA-MB-231 cells were treated with complexes **3** and **6** (at IC_{50} concentrations) for 24 h. The scale bar 20 μm.

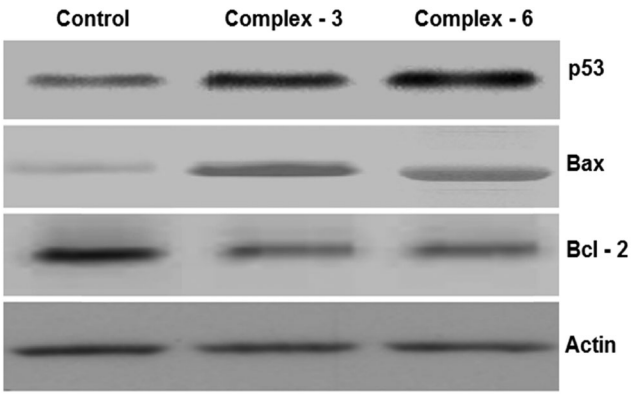

Fig. 9 Western blot of p53, Bax and Bcl-2 proteins in MDA-MB-231 cells. Lane-1 control samples, lanes-2 and 3 are samples treated with complexes **3** and **6** (at IC_{50} concentrations) respectively. β-Actin was used as the loading control.

apoptosis by **3** and **6** could be mediated through the downregulation of the antiapoptotic protein Bcl-2. The p53 and Bax protein levels in the MDA-MB-231 cancer cell lines are remarkably increased upon treatment with the complexes indicating that the complexes induce apoptosis (Fig. 9). Hence, the upregulation of proapoptotic protein Bax, p53 and the downregulation of antiapoptotic protein Bcl-2 caused by complexes **3** and **6** could possibly activate mitochondria-mediated apoptosis.[33]

Conclusions

An easy route for the synthesis of six new ruthenium(II) arene indole-3-carboxaldehye benzhydrazone complexes has been described here for the first time. The characterization of these complexes (**1–6**) was accomplished using analytical and spectroscopic methods (IR, UV-Vis, ^{1}H and ^{13}C NMR and ESI-MS). An X-ray diffraction study revealed that the benzhydrazone ligand coordinates to ruthenium *via* azomethine nitrogen and imidolate oxygen and adopts the familiar pseudo-octahedral "piano-stool" geometry. Interestingly, the cytotoxic activities of complex **6** against the tested cancer cell lines were significantly superior to that of the well-known anticancer drug cisplatin and the observed high cytotoxicity is correlated with the nature of the substituent of the ligand and arene moiety. Furthermore, fluorescence staining techniques and flow cytometry using the annexin-V assay revealed that complexes **3** and **6** induce apoptosis in MDA-MB-231 cancer cells. Furthermore, alkaline comet assays confirmed the single-strand break of DNA. The results of mitochondrial membrane potential and Western blot analysis demonstrated that the complexes with potent antiproliferative activity are able to induce mitochondria-mediated apoptosis in human cancer cells. On the basis of these results, we suggest that ruthenium arene benzhydrazone complexes may be the best candidates for further evaluation as chemopreventive and chemotherapeutic agents for human cancers.

Acknowledgements

One of the authors (MKMS) thanks the University Grants Commission (UGC), New Delhi for financial assistance through the UGC-BSR fellowship (Ref. no. F.7–22/2007(BSR)). We express sincere thanks to DST-FIST, India for the use of Bruker 400 MHz spectrometer at the School of Chemistry, Bharathidasan University, Tiruchirappalli-24.

References

1 L. Kelland, *Nat. Rev. Cancer*, 2007, **7**, 573–584.
2 (*a*) L. X. Cubeddu, I. S. Hoffmann, N. T. Fuenmayor and A. L. Finn, *N. Engl. J. Med.*, 1990, **322**, 810–816; (*b*) M. A. Jakupec, M. Galanski, V. B. Arion, C. G. Hartinger and B. K. Keppler, *Dalton Trans.*, 2008, 183–194.
3 P. J. Dyson and G. Sava, *Dalton Trans.*, 2006, 1929–1933.
4 G. Sava, A. Bergamo, S. Zorzet, B. Gava, C. Casarsa, M. Cocchietto, A. Furlani, V. Scarcia, B. Serli, E. Iengo, E. Alessio and G. Mestroni, *Eur. J. Cancer*, 2002, **38**, 427–435.
5 R. Trondl, P. Heffeter, C. R. Kowol, M. A. Jakupec, W. Berger and B. K. Keppler, *Chem. Sci.*, 2014, **5**, 2925–2932.
6 (*a*) A. L. Noffke, A. Habtemariam, A. M. Pizarro and P. J. Sadler, *Chem. Commun.*, 2012, **48**, 5219–5246; (*b*) R. E. Aird, J. Cummings, A. A. Ritchie, M. Muir, R. E. Morris, H. Chen, P. J. Sadler and D. I. Jodrell, *Br. J. Cancer*, 2002, **86**, 1652–1657; (*c*) G. Suss-Fink, *Dalton Trans.*, 2010, **39**, 1673–1688; (*d*) A. A. Nazarov, C. G. Hartinger and P. J. Dyson, *J. Organomet. Chem.*, 2014, **751**, 251–260; (*e*) R. Pettinari, F. Marchetti, C. Pettinari, A. Petrini, R. Scopelliti, C. M. Clavel and P. J. Dyson, *Inorg.*

Chem., 2014, **53**, 13105–13111; (*f*) L. E. H. Paul, B. Therrien and J. Furrer, *Inorg. Chem.*, 2012, **51**, 1057–1067; (*g*) M. Melchart, A. Habtemariam, O. Novakova, S. A. Moggach, F. P. A. Fabbiani, S. Parsons, V. Brabec and P. J. Sadler, *Inorg. Chem.*, 2007, **46**, 8950–8962; (*h*) R. K. Gupta, G. Sharma, R. Pandey, A. Kumar, B. Koch, P.-Z. Li, Q. Xu and D. S. Pandey, *Inorg. Chem.*, 2013, **52**, 13984–13996.

7 H. Chen, J. A. Parkinson, R. E. Morris and P. J. Sadler, *J. Am. Chem. Soc.*, 2003, **125**, 173–186.

8 A. Kurzwernhart, W. Kandioller, S. Bächler, C. Bartel, S. Martic, M. Buczkowska, G. Mühlgassner, M. A. Jakupec, H.-B. Kraatz, P. J. Bednarski, V. B. Arion, D. Marko, B. K. Keppler and C. G. Hartinger, *J. Med. Chem.*, 2012, **55**, 10512–10522.

9 W. Su, Q. Qian, P. Li, X. Lei, Q. Xiao, S. Huang, C. Huang and J. Cui, *Inorg. Chem.*, 2013, **52**, 12440–12449.

10 R. Pettinari, C. Pettinari, F. Marchetti, B. W. Skelton, A. H. White, L. Bonfili, M. Cuccioloni, M. Mozzicafreddo, V. Cecarini, M. Angeletti, M. Nabissi and A. M. Eleuteri, *J. Med. Chem.*, 2014, **57**, 4532–4542.

11 C. M. Clavel, E. Păunescu, P. Nowak-Sliwinska, A. W. Griffioen, R. Scopelliti and P. J. Dyson, *J. Med. Chem.*, 2015, **58**, 3356–3365.

12 Q. Wu, K. Zheng, S. Liao, Y. Ding, Y. Li and W. Mei, *Organometallics*, 2016, **35**, 317–326.

13 (*a*) T. Nasr, S. Bondock and M. Youns, *Eur. J. Med. Chem.*, 2014, **76**, 539–548; (*b*) T. Giraldi, P. M. Goddard, C. Nisi and F. Sigon, *J. Pharm. Sci.*, 1980, **69**, 97–98.

14 (*a*) M. Varache-Lembège, S. Moreau, S. Larrouture, D. Montaudon, J. Robert and A. Nuhrich, *Eur. J. Med. Chem.*, 2008, **43**, 1336–1343; (*b*) H. A. Abdel-Aziz, T. Aboul-Fadl, A.-R. M. Al-Obaid, M. Ghazzali, A. Al-Dhfyan and A. Contini, *Arch. Pharmacal Res.*, 2012, **35**, 1543–1552.

15 (*a*) M. Alagesan, P. Sathyadevi, P. Krishnamoorthy, N. S. P. Bhuvanesh and N. Dharmaraj, *Dalton Trans.*, 2014, **43**, 15829–15840; (*b*) E. Singleton and H. E. Swanepoel, *Inorg. Chim. Acta*, 1982, **57**, 217–221.

16 (*a*) J. Fernandez-de-Cossio, *Anal. Chem.*, 2010, **82**, 1759–1765; (*b*) IsoPro, version 3.1, Cornell University. A computer program written by Michael W. Senko that implements Yergey's polynomial method running under Microsoft Windows.

17 (*a*) M. A. Bennett and A. K. Smith, *J. Chem. Soc., Dalton Trans.*, 1974, 233–241; (*b*) M. A. Bennett, T. N. Huang, T. W. Matheson, A. K. Smith, S. Ittel and W. Nickerson, *Inorg. Synth.*, 1982, 74–78.

18 A. R. B. Rao and S. Pal, *J. Organomet. Chem.*, 2011, **696**, 2660–2664.

19 G. Sheldrick, *Acta Crystallogr., Sect. A: Found. Crystallogr.*, 2008, **64**, 112–122.

20 L. Farrugia, *J. Appl. Crystallogr.*, 1997, **30**, 565.

21 (*a*) R. J. Butcher, J. Jasinski, G. M. Mockler and E. Sinn, *J. Chem. Soc., Dalton Trans.*, 1976, 1099–1102; (*b*) R. N. Prabhu and R. Ramesh, *RSC Adv.*, 2012, **2**, 4515–4524.

22 K. N. Kumar, G. Venkatachalam, R. Ramesh and Y. Liu, *Polyhedron*, 2008, **27**, 157–166.

23 (*a*) M. U. Raja and R. Ramesh, *J. Organomet. Chem.*, 2012, **699**, 5–11; (*b*) M. Kalidasan, R. Nagarajaprakash, S. Forbes, Y. Mozharivskyj and K. M. Rao, *Z. Anorg. Allg. Chem.*, 2015, **641**, 715–723.

24 (*a*) F. Marchetti, C. Pettinari, R. Pettinari, A. Cerquetella, C. Di Nicola, A. Macchioni, D. Zuccaccia, M. Monari and F. Piccinelli, *Inorg. Chem.*, 2008, **47**, 11593–11603; (*b*) D. Pandiarajan and R. Ramesh, *J. Organomet. Chem.*, 2013, **723**, 26–35.

25 (*a*) J. Valladolid, C. Hortiguela, N. Busto, G. Espino, A. M. Rodriguez, J. M. Leal, F. A. Jalon, B. R. Manzano, A. Carbayo and B. Garcia, *Dalton Trans.*, 2014, **43**, 2629–2645; (*b*) F. Aman, M. Hanif, W. A. Siddiqui, A. Ashraf, L. K. Filak, J. Reynisson, T. Söhnel, S. M. F. Jamieson and C. G. Hartinger, *Organometallics*, 2014, **33**, 5546–5553; (*c*) X. Lei, W. Su, P. Li, Q. Xiao, S. Huang, Q. Qian, C. Huang, D. Qin and H. Lan, *Polyhedron*, 2014, **81**, 614–618.

26 (*a*) A. Habtemariam, M. Melchart, R. Fernández, S. Parsons, I. D. H. Oswald, A. Parkin, F. P. A. Fabbiani, J. E. Davidson, A. Dawson, R. E. Aird, D. I. Jodrell and P. J. Sadler, *J. Med. Chem.*, 2006, **49**, 6858–6868; (*b*) R. E. Morris, R. E. Aird, P. del Socorro Murdoch, H. Chen, J. Cummings, N. D. Hughes, S. Parsons, A. Parkin, G. Boyd, D. I. Jodrell and P. J. Sadler, *J. Med. Chem.*, 2001, **44**, 3616–3621.

27 (*a*) L. He, S.-Y. Liao, C.-P. Tan, R.-R. Ye, Y.-W. Xu, M. Zhao, L.-N. Ji and Z.-W. Mao, *Chem. – Eur. J.*, 2013, **19**, 12152–12160; (*b*) Q. Wu, C. Fan, T. Chen, C. Liu, W. Mei, S. Chen, B. Wang, Y. Chen and W. Zheng, *Eur. J. Med. Chem.*, 2013, **63**, 57–63; (*c*) Q. Wu, K. Zheng, S. Liao, Y. Ding, Y. Li and W. Mei, *Organometallics*, 2016, **35**, 317–326.

28 R. K. Gupta, R. Pandey, G. Sharma, R. Prasad, B. Koch, S. Srikrishna, P.-Z. Li, Q. Xu and D. S. Pandey, *Inorg. Chem.*, 2013, **52**, 3687–3698.

29 (*a*) Z.-F. Chen, Q.-P. Qin, J.-L. Qin, Y.-C. Liu, K.-B. Huang, Y.-L. Li, T. Meng, G.-H. Zhang, Y. Peng, X.-J. Luo and H. Liang, *J. Med. Chem.*, 2015, **58**, 2159–2179; (*b*) J. P. Johnpeter, G. Gupta, J. M. Kumar, G. Srinivas, N. Nagesh and B. Therrien, *Inorg. Chem.*, 2013, **52**, 13663–13673.

30 B. Banik, K. Somyajit, G. Nagaraju and A. R. Chakravarty, *Dalton Trans.*, 2014, **43**, 13358–13369.

31 R. M. Lord, A. J. Hebden, C. M. Pask, I. R. Henderson, S. J. Allison, S. L. Shepherd, R. M. Phillips and P. C. McGowan, *J. Med. Chem.*, 2015, **58**, 4940–4953.

32 (*a*) C. Qian, J.-Q. Wang, C.-L. Song, L.-L. Wang, L.-N. Ji and H. Chao, *Metallomics*, 2013, **5**, 844–854; (*b*) R. Cao, J. Jia, X. Ma, M. Zhou and H. Fei, *J. Med. Chem.*, 2013, **56**, 3636–3644.

33 (*a*) A. J. Levine, J. Momand and C. A. Finlay, *Nature*, 1991, **351**, 453–456; (*b*) J. C. Reed, *J. Cell Biol.*, 1994, **124**, 1–6; (*c*) T. Chen, Y. Liu, W.-J. Zheng, J. Liu and Y.-S. Wong, *Inorg. Chem.*, 2010, **49**, 6366–6368.